Solid State Lighting Program

Final Report

High Quantum Efficiency OLED Lighting Systems

Work Performed Under Agreement: **DE-FC26-07NT43226**

Submitted By:
General Electric Global Research

Principal Investigator:

Joseph Shiang

GE Global Research

1 Research Circle, Room K1-3B41A

(518)-387-6550 shiang@ ge.com

High Quantum Efficiency OLED Lighting Systems

Report prepared by: Joseph Shiang and Paul Smigelski

Summary:

The overall goal of the program was to apply improvements in light outcoupling technology to a practical large area plastic luminaire, and thus enable the product vision of an extremely thin form factor high efficiency large area light source. The target substrate was plastic and the baseline device was operating at 35 LPW at the start of the program. The target LPW of the program was a >2x improvement in the LPW efficacy and the overall amount of light to be delivered was relatively high 900 lumens. Despite the extremely difficult challenges associated with scaling up a wet solution process on plastic substrates, the program was able to make substantial progress. A small molecule wet solution process was successfully implemented on plastic substrates with almost no loss in efficiency in transitioning from the laboratory scale glass to large area plastic substrates. By transitioning to a small molecule based process, the LPW entitlement increased from 35 LPW to 60 LPW. A further 10% improvement in outcoupling efficiency was demonstrated via the use of a highly reflecting cathode, which reduced absorptive loss in the OLED device. The calculated potential improvement in some cases is even larger, ~30%, and thus there is considerable room for optimism in improving the net light coupling efficacy, provided absorptive loss mechanisms are eliminated. Further improvements are possible if scattering schemes such as the silver nanowire based hard coat structure are fully developed. The wet coating processes were successfully scaled to large area plastic substrate and resulted in the construction of a 900 lumens luminaire device.

I. Introduction

A key limiting factor in OLED energy efficiency is the relatively low external quantum efficiency (EQE), the ratio of emitted photons to injected charge carriers. Since the energy efficiency of a device is the product of the EQE with all the other energy loss terms in the device, the EQE value determines the upper limit of the device energy efficiency. Given typical white light OLED operating voltages and color characteristics, an EQE of ~50% is required to match the mercury fluorescent technology's 30% energy efficiency and 100 LPW performance.

It is generally recognized that there are two fundamental conditions that must be met for an OLED to have high EQE: 1) All the charges must recombine inside the device to form an emissive state. The efficiency of this process is the internal quantum efficiency or IQE. 2) The light generated by the emissive state must be extracted from the OLED active layers to the air. Considerable effort has been devoted to both of these aspects of the problem, and there now exist OLED devices that have IQE values approaching unity, and a number of light extraction schemes have been reported.

The goal of the program was to substantially increase the light extraction efficiency from flat planar OLED devices prepared via solution processing. While it is relatively easy to increase light extraction from a point coupled into a shaped substrate (lens shaped LED's having been proposed since the 1960's) it is much more difficult to couple light from a large planar emitter. In addition, from a product development point of view, it is important that any successful OLED outcoupling scheme operates on large area planar substrates. From a manufacturing and product point of view, it is important that the outcoupling approaches are consistent with solution deposition of the organic layers, and are compatible with processing on large flexible plastic sheets. The GE vision for the lighting product that would be enabled by the work of this project is shown in figure 1. Achieving these goals requires optimization of both the light outcoupling at the device level through design modifications and the implementation of the designs on large area plastic substrates. Despite the considerable technical difficulty inherent in both of these aspects, considerable progress was made, and by the program's end a large area 900 lumens multi-panel luminaire using plastic substrates was prepared. The cohort of panels used to construct the luminaire had average initial performance of 45 LPW and an average color temperature of 3050 K. For the OLED design used in the luminaire, the laboratory performance closely matched that of the small scale performance on glass. The flexible panels were integrated onto a single 3/32" Lexan (TM) sheet to form a conformable luminaire. The picture of a section of the luminaire is shown in the bottom of figure 1.

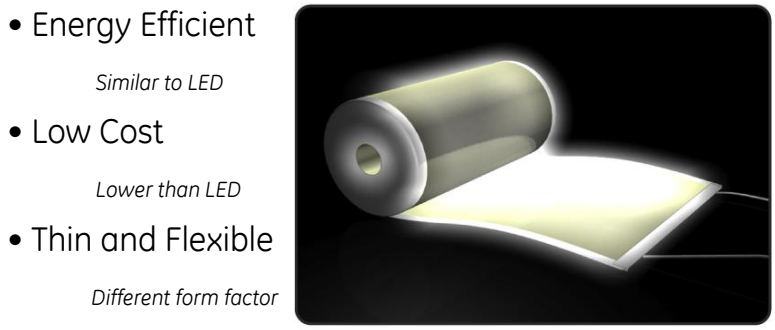

Figure 1: An OLED product vision for an energy efficient, low cost light source with a thin, flexible form factor.

Figure 2: The large area, 900 lumen, thin and flexible luminaire delivered by this project

II. Program Rationale.

The program is guided by the team's understanding of the detailed optical physics of the OLED structures. It is appropriate, before a discussion of the program tasks, to present a detailed discussion of what optical models reveal about the light propagation within OLEDs.[1] Understanding the amount of light extraction that can be expected requires the use of optical models of the thin film device structure. These models take into account interference effects that occur when an emitter is placed into a cavity whose dimensions are on the order of the emission wavelength. For planar structures these models readily predict the detailed angular emission pattern of the OLED. This angular distribution profile can be integrated over selective regions to calculate the relative amount of energy that is coupled into the air, trapped in the waveguide modes of the substrate or active device layers (i.e. the ITO and organic layers), or trapped into the lossy plasmon modes of the metal cathode[2]. Table 1 presents the results of such a calculation for a typical OLED device structure.

The calculation is based on a model built by McGehee et. al. and requires as input parameters the complex index of refraction for each layer along with the orientation of the emitting dipoles of the device relative to the plane of the OLED structure.[3] Dipoles that are oriented perpendicular to the plane of the OLED couple most efficiently to the active layer waveguide modes and cathode plasmon modes of the device and least efficiently to the air. Thus, this particular orientation is highly undesirable. Conversely, dipoles that are oriented along the plane of the OLED couple very inefficiently to the active layer and cathode modes and most efficiently into the air. Dipoles that have random orientation are intermediate

---

[1] Much of this discussion in drawn from A.R. Duggal, C.M. Heller, J.J. Shiang, J. Liu, L.N. Lewis"Solution-processed organic light-emitting diodes for lighting", *IEEE/OSA Journal of Display Technology* 3 (2), pp. 184-192, 2006

[2] W. L. Barnes, "Electromagnetic crystals for surface plasmon polaritons and the extraction of light from emissive devices", *IEEE J. Lightwave Tech.*, vol. 17, pp. 2170-2182, Nov. 1999; R. R. Chance, A. Prock, and R. Silbey, *Adv. in Chem. Phys.*, vol. 37, pp 1-65, 1978.

[3] J. M. Ziebarth, M. D. McGehee, A theoretical and experimental investigation of light extraction from polymer light-emitting diodes, *J. Appl. Phys.*, vol. 97, pp. 064502-1, 064502-7, Mar. 2005.

between these two extreme cases. Fortuitously, many electroactive polymer materials have a linear, rod like structure which naturally tend to align along plane of the OLED. Devices that utilize these materials typically have relatively high output coupling to the air. This stands in sharp relief to OLEDs whose emitters are based upon randomly oriented dipoles[4].

Table 1 shows the results for two separate calculations – one for the dipoles with an isotropic angular distribution and one for the dipoles all aligned along the plane of the interface. The results show that for an isotropic dipole distribution in this device structure only 26% of the light makes it out of the device as compared to 44% for the in-plane dipole distribution. This indicates that there is more to be gained in improving outcoupling efficiency for a device which utilizes a isotropically small-molecule dye emitter than for one which utilizes a conjugated polymer emitter. The results also indicate that different outcoupling schemes need to be employed for the two different dipole distributions. For instance, for the isotropic distribution, it is most worthwhile to develop schemes that extract energy lost in plasmon modes at the cathode[5] since this is the major source of loss whereas for the in-plane distribution, such schemes would be of secondary importance.

The results presented in Table 1 assume that the emission zone is located at an optimal position relative to all the other dielectric layers and interfaces in the device. An additional insight of these optical models is that in a standard OLED, the output coupling efficiency to the air is a sensitive function of the location of the emission zone.[4] Thus, careful adjustment of the thickness of the device layers is an absolute imperative. In vapor deposited OLEDs this is achieved via adjusting the thickness of the various transport layers of the multilayer device[6] whereas for solution processed devices this is achieved by adjusting the material composition of the layer(s) to achieve an optimal charge balance and recombination zone position

Table 1: Partitioning of light in a typical OLED structure, assuming no absorptive loss. The results were obtained by calculating over the angular distribution inside the OLED to calculate the relative amount of energy that is coupled into the air, trapped in the waveguide modes of the substrate or active device layers (i.e. the ITO and organic layers), or trapped into the lossy plasmon modes of the metal cathode

	Isotropic Dipole Distribution	In-Plane Dipole Distribution
Useful Light (Air Modes)	26%	44%
Trapped in Active Layers	12%	8%
Trapped in Cathode	35%	8%
Trapped in Substrate	27%	40%

Even with careful optimization of the emissive layers, a significant amount of light is trapped in the substrate for both the isotropic and in-plane dipole distributions and for both cases Table 1 shows that an approximately 2X enhancement is possible. Since the structure and shape of the substrate can be

[4] C M Ramsdale and N C Greenham, "The optical constants of emitter and electrode materials in polymer light-emitting diodes", *J. Phys. D: Appl. Phys*., vol. 36, pp. L29-L34, Jan. 2003.
[5] J. M. Lupton, B.J. Matterson, I.D.W. Samuel, M.J. Dory, W.L. Barnes, "Bragg scattering from periodically microstructured light emitting diodes" *Appl. Phys. Lett*., vol. 77, pp. 3340-3342, Nov. 2000.
[6] V. Bulovic, V.B Khalifin, G. Gu, P.E. Burrows, D.Z. Garbuzov, and S.R. Forrest, "Weak microcavity effects in organic light-emitting devices", *Phys. Rev. B*., vol. 58, pp. 3730-3740, Aug. 1998.

modified without affecting the performance of the active layers of the OLED, there are numerous possible methods to extract light that is trapped within substrate modes[7]. For lighting, where maintaining low cost is critical, the scheme of simply applying a scattering layer on top of the device is quite promising.[8]

The structure of the program proceeds directly from our prior modeling and experimental results. In the program, we refined our existing models, and apply them directly to particular systems of interest. (Task 1- Build and Verify Numerical Model of Complete OLED System). We also the improve EQE in actual devices by 1) reducing the amount of light that is coupled into the cathode by modifying the electrode structure or the emission characteristics of the OLED and by 2) (Task 2 - Modify OLED Active Layers to Increase EQE) optimizing the extraction efficiency from the large area plastic substrate by using optimal cathode design and other light enhancement methods. (Task 3- Optimize Light Extraction Architecture). Construction and incorporation of the solution processed OLED panels was the final technical task of program. (Task4 - Produce Integrated Product Prototype) While our initial results would tend to favor devices with aligned emitters, we stress that the combination of modeling and experimental work in this program will be effective whether the emitter is aligned or is randomly oriented.

The overall task structure and relations of the tasks to one another is shown in Figure 3. The overall progress of the program as it proceeded through the task structure is shown in Figure 4. Three major milestones of the program are indicated. First the team was able to transition from glass to plastic, which despite some initial performance reduction, was a critical demonstration that all the necessary process steps could be manufactured on plastic substrates using solution processing.

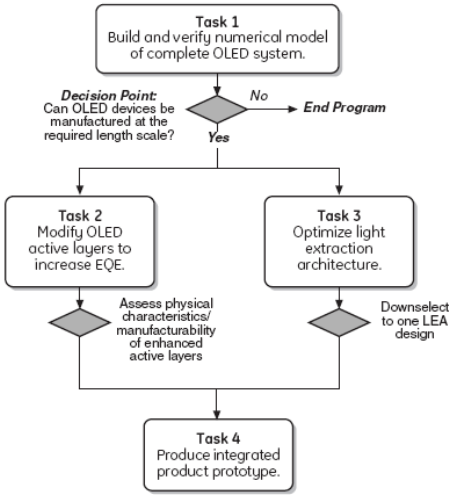

Figure 3: PERT diagram illustrating the relationship between the program tasks.

---

[7] S. Möller, S. F. Forrest, "Improved light out-coupling in organic light emitting diodes employing ordered microlens arrays", *J. Appl. Phys*., vol. 91,pp. 3324-3327 ,Mar. 2002; G. Gu, D. Z. Garbuzov, P.E. Burrows, S. Venkatesh, S. R. Forrest, M. E. Thompson, "High-external-quantum-efficiency organic light-emitting devices", *Optics Letters*, vol. 22, pp. 396-398, Mar. 1997; C. F. Madigan, M. H. Lu, and J. C. Sturm, "Improvement of output coupling efficiency of organic light-emitting diodes by backside substrate modification", *Appl. Phys. Lett.* vol. 76, pp. 1650-1652, Mar. 2000.; T. Tsutsui, M. Yahiro, H. Yokogawa, K. Kawano, M. Yokoyama,"Doubling coupling-out efficiency in oraganic light emtting devices using a thin silica aerogel layer" , *Adv. Mat.*, vol. 13, pp. 1149-1152 , Aug. 2001; T. Yamasaki, K. Sumioka, T. Tsutsui, "Organic light-emitting device with an ordered monolayer of silica microspheres as a scattering medium", *Appl. Phys. Lett*, vol. 76, pp. 1243-1245, Mar. 2000.

[8] J. J. Shiang, A. R. Duggal, "Application of radiative transport theory to light extraction from organic light emitting diodes", J. Appl. Phys., vol. 95, pp. 2880-2888 Mar. 2004; J. J. Shiang, T. J. Faircloth, A. R. Duggal, "Experimental demonstration of increased organic light emitting device output via volumetric light scattering" ,*J. Appl. Phys.*, vol. 95, pp. 2889-2895, Mar. 2004.

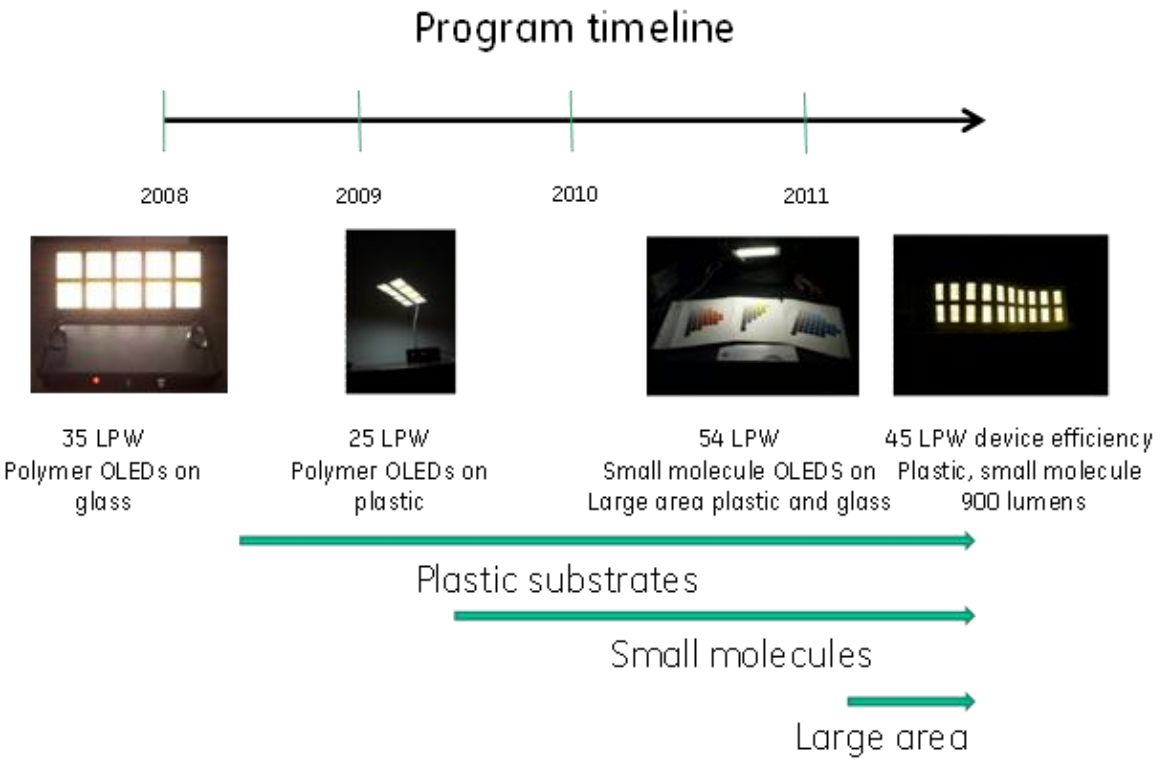

Figure 4: Time line of program activities showing starting point, different intermediate points and technical activities

III. Technical Activities

Task 1

The optical extraction efficiency, η_{ex}, was separated into two components: the injection efficiency from the active layers into the substrate $\eta_{OLED\text{-}s}$, and the extraction efficiency from the substrate to the ambient $\eta_{s\text{-}a.}$ i.e. $\eta_{ex} = \eta_{OLED\text{-}s}\, \eta_{s\text{-}a}$. To calculate $\eta_{OLED\text{-}s}$ we used a microcavity model, and to calculate $\eta_{s\text{-}a}$ we used an optical scattering model that was developed under a prior DOE contract DE-FC26-00NT40989.

The microcavity model used in the program had explicit equations for the rate of decay and measured angular emission profile for a dipole placed between two multilayer mirrors. (see figure 5) The model also included a method for evaluating the loss due to the presence of absorption in one or more dielectric layers, the relative partitioning of top and bottom emission in transparent OLEDs and effect of optical anisotropy on these quantities. The model used the CPS results for a dipole embedded in a medium (medium 1) that in turn is sandwiched between two infinite media (2 and 3) with different dielectric characteristics. We calculated the total amount of energy transferred across each interface from medium 1. The model thus explicitly included the effect of absorptive loss from materials used in the OLED and in the cathode. In the model, each of the interfaces could be a multilayer structure, whose net dielectric properties could be calculated via a transfer matrix formalism. The model also calculated the angular emission profile and provided a means of extending the results to encompass anisotropic media.

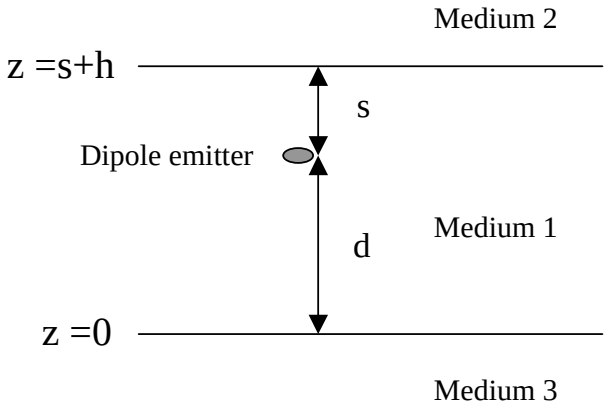

Figure 5: Microcavity geometry of a dipole emitter between two infinite parallel plates. The distance between the emitter and the boundaries is set by the parameters s and d.

The scheme we have developed to provide a complete optical model of the OLEDs is shown below (Figure 6). The required inputs into each component of the model are shown in green. The solid boxes highlight the fundamental physical characteristic of each class of inputs. Thus the microcavity model allows one to establish a relationship between the internal quantum efficiency and output characteristics of the unmodified device, and the scattering model connects the scattering characteristics of the substrate to the total quantum efficiency following the enhancement. Commercially available ray tracing tools, which are complimentary to radiative transport models, were used to model some specific substrate structures. The file system used in the modeling chain has been designed to permit facile connection between all the various modeling components.

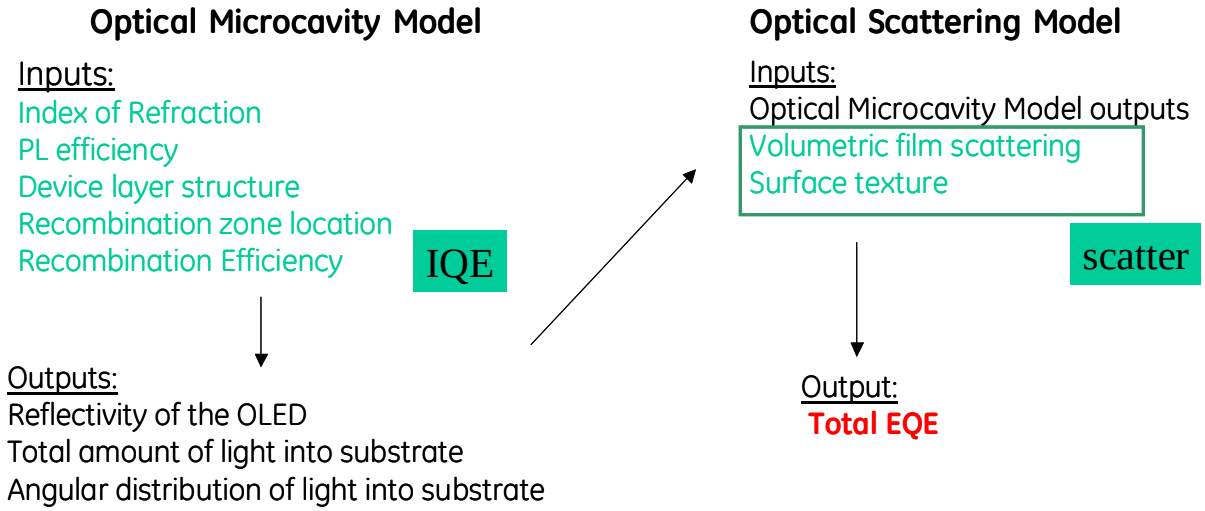

Figure 5 A schematic diagram of the modeling approach used by the program

The importance of an integrated approach that considers both $\eta_{OLED\text{-}s}$ and $\eta_{s\text{-}a.}$ is shown in Figure 7. A commonly used metric to assess the efficiency of a light outcoupling scheme is to use an "enhancement factor", typically the ratio of the EQE with the treatment ratio to the EQE of the OLED without the treatment. While the measurement is relatively straight forward, the results presented in the figure demonstrates why this is a particularly poor metric. In the examples shown in the figure, the OLEDs differ in the angular distribution of the light that is coupled from the OLED into the substrate. In the case considered on the left of the figure (Case A), the light that emerges from the OLED and goes into the substrate is largely forward directed. In the case considered on the right (Case B), a Lambertian distribution emerges from the OLED. In the absence of any additional light coupling enhancement the fraction of light coupled from the substrate into the ambient is 0.62 in Case A and 0.38 in Case B. For both cases the same scattering film is applied and the net light outcoupling computed using the Optical Scattering model. In case A the scattering film improved the net light coupling only modestly, by a factor of 1.18X, in the second case the improvement is much larger, 1.63X. The OLED of Case A, however, has better light output (0.73) than the OLED of Case B (0.68), opposite to what is suggested by the film "enhancement factor" This simple demonstration illustrates that *estimations of EQE improvements based upon an "enhancement factor" are simply not valid*. During the course of the program this false metric was scrupulously avoided and all results are presented in terms of a calculated total efficiency (for theoretical result) or an actual measured EQE (for an experimental result).

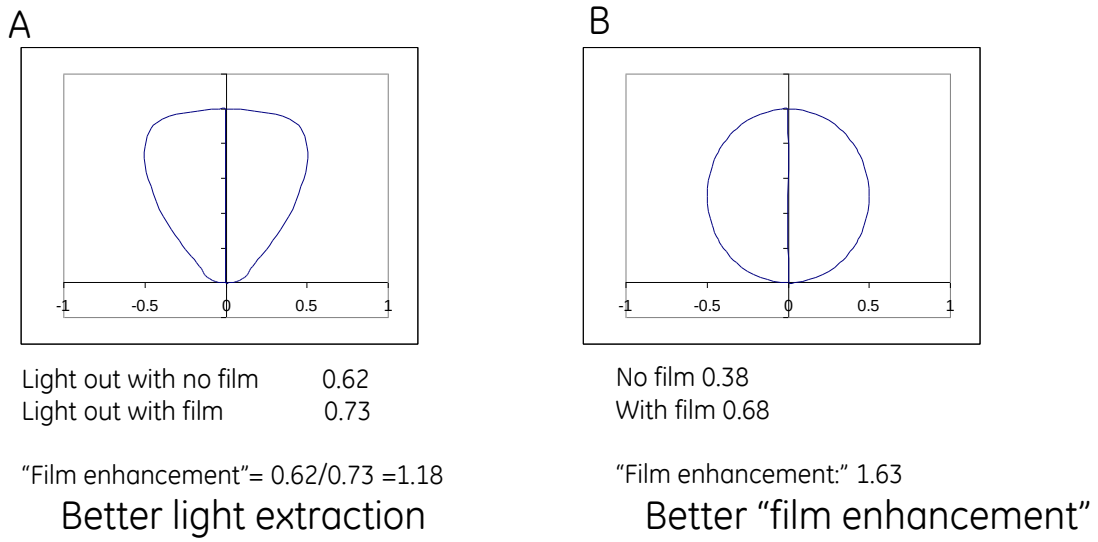

Figure 6 Two different cases for light extraction efficiency using a scattering film. Case A (right) considers the film coupled to an OLED with a highly forward directed emission. After the application of the film, the overall light extraction efficiency in this case is 0.73. Case B considers the same film coupled to and OLED with a Lambertian emission patters. In this case, after application of the film the light extraction efficiency is 0.68.

Task 2

A number of schemes to increase the light output from OLED devices have been proposed. Most schemes involve texturing or patterning one or more interfaces or layers in the OLED to scatter light. Patterning the substrate allows for light that has been trapped in the substrate to be extracted and increase the total light extraction but does not affect the amount of light that been lost due to coupling to the cathode of the device. An issue with incorporation of scattering centers in the active layers of the OLED is that the additional morphology makes it harder to form the continuous layers needed to prevent device shorting and leakage.

One possible approach to increase the amount of light coupled from the OLED into the substrate is to increase the optical index of the substrate that supports the transparent anode material. This approach has the advantage that it does not necessarily affect the smoothness of the anode. For example, increasing the optical index of the substrate from n=1.5 to n =1.8 can increase the amount of light coupled into the substrate by a factor of 1.5. The problem then becomes the increased difficultly of extracting this light from the higher index substrate. It is thus necessary to compliment the use of a high index substrate with some degree of light scattering without affecting the smoothness. In this manner the optical properties of the OLED active layers are effectively modified in a manner that does not affect the ability to form continuous, pinhole free organic films.

In the program, the use of silver nanowire/polymer composite material to enable both increasing the effective optical index of the substrate and providing a means of extracting light from the high index was explored. The approach that was pursued was to coat a substrate with an optically thick (i.e. several microns) transparent high index film that also provides a smooth, chemically resistant surface that is suitable for further solution based fabrication of an OLED device. Within this layer, high aspect ratio Ag nanowires were used to scatter light that would normally be waveguided and remain within the device. In this section, a detailed description of the synthesis of the high aspect ratio nanowires and the formation of

the nanowire/high index composite smooth polymer films is provided. Some preliminary results that show that these films exhibit promising optical properties and are compatible with many of the fabrication steps required to fabricate solution processed OLEDs are also presented.

Experimental

General Methods. Silver nitrate (ACS reagent grade), polyvinylpyrrolidone, benzenethiol and acryloyl chloride were purchased from Sigma-Aldrich and used without further purification. Sodium chloride, acetone, isopropanol and toluene were purchased from Fisher Chemical and used without further purification. Epichlorohydrin was purchased from Alfa Aesar and used without further purification. Ethylene glycol was purchased from Fisher Chemical and was fractionally distilled prior to use collecting the fraction with a boiling point of 195 °C.

Scanning electron microscope images were acquired with either a Hitachi SU-70 or Zeiss Supra 55VP scanning electron microscope with an accelerating voltage of 5kV, using a working distance of approximately 5 mm for all of the samples. The SEM images were analyzed using Clemex Vision image analysis software. The images were first enhanced to increase the contrast between the nanowires and the background. The grey level SEM image was then transformed into a binary image (white-nanowires, black-background) using the characteristic grey level range of the nanowires that were basically white relative to the background color. In order to measure the lengths of the nanowires, the Clemex Vision software separated clumped nanowires using the linear nature of the nanowires where possible. In addition to the automated separation of nanowire clumps, some manual separation was used when needed in order to ensure that all of the nanowires in each SEM image were measured. 5kX SEM images were used to measure the nanowire lengths and a 50kX magnification to measure the nanowire thickness. The thickness was measured in a similar manner using the same segmentation procedure. Once the binary image was created the Clemex Vision software automatically measured the thickness every 10 nanometers along the length of the nanowires.

Surface characterization was done using AFM and optical profilometetry. Surface roughness values and AFM images were generated using a Veeco (Santa Barbara, CA) Dimension 3000 SPM instrument equipped with a Nanoscope IV controller. The SPM instrument was set up in tapping mode and a TESP AFM tip (Veeco, Santa Barbara, CA) was used. Optical profilometry measurements were performed on a MicroXAM (KLA Tencor Corporation, Tucson, AZ) optical surface profiler using a 10X objective lens and a 1X analog magnification factor, to result in an imaging area of 816 x 618 μm^2. The image data was post-processed to remove tilt and long-range curvature, prior to data analysis. Both 2D and 3D images, and x and y line scans were created with a SPIP™ software package (Image Metrology A/S, Horsholm, Denmark). The sample was prepared for OP experiments by evenly depositing 5 nm of Pt onto the surface with an Emitech K575X (West Sussex, United Kingdom) sputter coater. The platinum coating was necessary to reduce the transparency of the sample so it would be amenable to OP imaging. The absorption spectra were recorded using a Varian Cary 300 Scan UV-Visible spectrophotometer. Emission spectra were recorded by excitation at either 380 or 410 nm using an Edinburg Analytical Instruments CD920. Optical microscopy images were taken using a Zeiss microscope and Qimaging camera. NMR spectra were recorded using a Bruker Avance 400 MHz NMR. The refractive index of the cured films was measured using a Metricon Prism Coupler with a red laser emitting at 632.8 nm.

Synthesis and purification of bisPTEA (1,3-bis(phenylthio)propan-2-acrylate)

bisPTE (1,3-bis(phenylthio)propan-2-ol). To a 3-liter flask, equipped with a mechanical stirrer, an addition funnel, a water-jacketed condenser and nitrogen sparge, was added one liter of toluene. The flask was purged well with nitrogen, and benzenethiol (183 ml, 1.78 moles) and epichlorohydrin (69.8 mL, 0.892 mole) were added via syringe. In a separated Erlenmeyer flask, potassium hydroxide (61 g, 0.957 mole) was dissolved in one liter of isopropanol. Once the KOH was fully dissolved, the solution added at a steady rate to the round-bottomed flask. Upon completion of the addition the solution was brought to reflux for one hour and forty minutes. The heat was turned off, and the reaction was allowed

to stir over the weekend. A ^{1}H NMR revealed complete reaction of the epichlorohydrin. The reaction was neutralized with HCl and then washed three times with dilute $HCl_{(aq)}$. This was followed by three washes with dilute bicarbonate solution and five washes with deionized water until the pH was 6-8. The organic phase was then dried over $MgSO_4$, and the solvents were removed by rotary evaporation. The final yield was 249.9g, which was slightly more than theory due to residual solvent. ^{1}H NMR (400 MHz, $CDCl_3$) δ 3.00-3.30 (m, 4H), 3.90 (m, 1H), 7.15-7.45 (m, 10H).

bisPTEA (1,3-bis(phenylthio)propan-2-acrylate). To a 3-liter flask, equipped with a mechanical stirrer, an addition funnel, a water-jacketed condenser and nitrogen sparge, was added one liter of toluene. Acryloyl chloride (80 mL, 0.985 mole) was added to the toluene. Into the addition funnel were added 1,3-bis(phenylthio)propan-2-ol (248 g, 0.897 mole) and triethylamine (99.7 g, 0.985 mole) as a solution with 500 mL of toluene. The alcohol solution was slowly added to the flask to keep the exotherm under control. Once the addition was complete the reaction was brought to reflux for 15 minutes and then the heat was turned off. The reaction was then left to stir overnight. A ^{1}H NMR revealed complete reaction of the alcohol. The reaction was diluted with diethyl ether to precipitate the amine hydrochloride salt and was filtered through a course-fritted funnel. The clear yellow solution was washed with dilute $HCl_{(aq)}$ three times to remove any residual amine. An additional three washes with dilute potassium hydroxide and then four washes with deionized water returned the pH to between 6 and 8. The organic layer was dried over $MgSO_4$ and the solvents were removed by rotary evaporation. Twenty milligrams of MEHQ were added to the flask to inhibit polymerization. ^{1}H NMR (400 MHz, $CDCl_3$) δ 3.30 (m, 4H), 5.21 (m, 1H), 5.80 (d, 1H), 5.98 (q, 1H), 6.27 (d, 1H), 7.15-7.45 (m, 10H).

Purification of bisPTEA (1,3-di(thiophenyl)-2-propylacrylate). The optimal procedure was determined to be dissolution of the acrylate in hexanes with stirring. A small amount of dark precipitate forms from which the hexane solution is decanted and filtered through a 4 inch thick pad of silica gel 3 inches in diameter. The silica was washed with hexanes until no further product came off when analyzed by TLC. The solvent was removed by rotary evaporation with 20 mg of MEHQ to inhibit polymerization after which a slight haze appeared. This was removed by filtration through a 0.45 micron filter.

Prepartion of silver nanowires.

Large scale synthesis of silver naowires. Silver nanowires were prepared using a modified version of the procedure used by Sun and Xia.[9] Ethylene glycol used in all the solutions and as the reaction solvent was fractionally distilled throwing away the leading fraction with a boiling point below 195 °C. Silver nitrate solution (0.30 M) in ethylene glycol was prepared and stored in a plastic bottle in the dark. Sodium chloride solution (6.7 mM) in ethylene glycol was prepared and stored in a plastic bottle. Poly(vinypyrrolidone), (mw = 55k or 1M) was dissolved in 5 grams ethylene glycol to which 2 mL of NaCl solution had been added and then the total solution mass adjusted to 8.33 grams. Ethylene glycol (150 mL) was heated to 160 °C in a 250 mL round bottomed flask, sparged with an atmosphere of nitrogen and stirred magnetically. Once heated 10 mL of the silver nitrate solution and 5 mL the PVP solution were injected into the flask from separate syringes at a rate of 0.6 mL/min, based on the volume of silver nitrate solution, using a dual-channel syringe pump. Once the injection was complete the syringes were removed from the flask and the reaction left to stir for 1 hour under a blanket of nitrogen. Over the course of the reaction the solution slowly darkened until it became opaque and opalescent. After the hour, the reaction was removed from the heat and transferred to a plastic bottle to cool.

Isolation and characterization of silver nanowires. A 5 mL aliquot of the cooled silver solution was diluted with acetone causing the silver wires to precipitate. The wires were collected and washed 3 times with isopropanol to remove excess PVP, collecting the wires by centrifugation and decanting the clear supernatant between each wash. The silver wire concentrate was diluted to 2 mL with isopropanol and characterized by UV/Vis and SEM.

Preparation of silver nanowires for coating. A 10 mL portion of the cooled silver solution was centrifuged and the supernatant discarded. The silver wire concentrate was dispersed in isopropanol to make a 2 mL solution.

Preparation of hardcoat resin. The hardcoat was prepared by blending equal parts of the monomers bisPTEA and RDX 51027 at 50 °C with gentle shaking. Once fully blended Irgacure 819 photocatalyst (1 wt%) was added and dissolved by continued shaking at 50 °C. The silver nanowire dispersion was then added to the blend (10% v/w). The nanowires were dispersed in the viscous blend by gentle mixing with a spatula and the resin was degassed under vacuum to remove the residual iso-propanol and any air bubbles.

Preparation of small samples by molding. Substrates of either 1" x 1" glass or plastic squares were rinsed with isopropanol and dried under a stream of nitrogen. Acrylate resin doped with silver nanowires was added to one side of the substrate and compression molded against a silicone mold. The resin was then cured using a Xenon flash photolysis apparatus. The lamps were set at the minimum height and the sample cured using three 10-second exposures allowing the sample to cool between exposures. The substrate and cured resin coating was then released from silicone mold. Fluorescent polymer BLUE was then applied to the coated side of the substrate by spin-coating a 1% solution in toluene at 300 rpm for 30 seconds.

Preparation of large samples by lamination. Plastic substrates (7" x 7") were cleaned with a static roller. A bead of approximately 1 mL of resin was deposited along one edge of the plastic. The plastic square was then aligned with a 6" x 6" silicone mold and affixed with adhesive tape. Passage of the article through a laminator gave a uniform coating deposited between the substrate and mold. The mold was then transferred to a belt driven Fusion UV-cure line. The mold was passed under the lamps three to five times and then let cool. Once cooled the substrate with coating was released from the mold and passed under the lamps twice more with the resin side facing the lamps. Excess resin and uncoated substrate were trimmed away to provide an article approximately 5" x 5". Small samples were then cut as needed and coated with either fluorescent resin or ITO.

Results and Discussion

Our initial attempts to reproduce the preparation of silver nanowires as described by Sun and Xia[9] met with limited success, producing only solutions containing nanoparticles or nanorods when we used a 0.60 M PVP injection solution. Reactions at this concentration of PVP gave a broad absorption maximum centered at 409 nm and extending down to 385 nm rather than the distinct peak around 380 nm characteristic of a pure nanowire solution. (Figure 8) It is well known that the ratio of the surfactant polymer polyvinylpyrrolidone (PVP) to silver nitrate is critical to attaining selective nanowire growth. Optimizing the synthesis by changing the PVP/Ag ratio failed to give selective nanowire formation. These reactions never achieved the opalescence indicative of a nanowire solution nor did the UV/Visible spectrum from these reactions show the expected plasmon absorption band at 380-400 nm. The measured absorption maximum near 430 nm was more indicative of nanoparticles and nanorods.[10] The lower PVP concentration reactions also produced a large amount of agglomerated silver.

---

[9] Sun, Y.; Xia, Y. *Adv. Mater.* **2002,** *14,* 833.

[10] (a) Sun, Y.; Gates, B.; Mayers, B.; Xia, Y. *Nano Lett.* **2002,** *2,* 165. (b) Kerker, M. *J. Colloid Interface Sci.* **1985,** *105,* 297. (c) Dickson, R. M.; Lyon, L. A. *J. Phys. Chem. B.* **2000,** *104,* 6095. (d) Sarkar, D.; Halas, N. J. *Phys. Rev. E.* **1997,** *56,* 1102

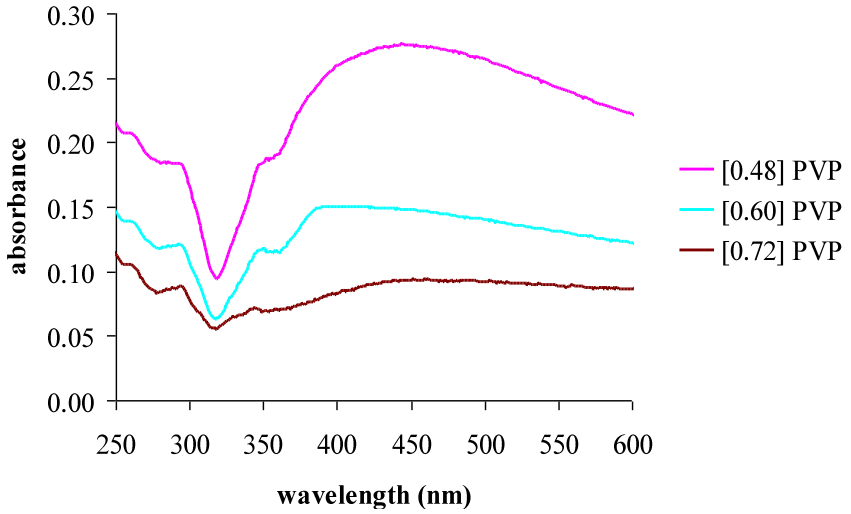

Figure 7 Effect of PVP injection concentration on absorption spectrum

A reexamination of the more recent literature revealed that careful control of temperature[10a], atmosphere, PVP concentration[9,11] , addition rate, and the presence of added salts[12,13,14] were all generally considered to be critical in controlling the morphology of the nanoparticle. The resulting morphologies include twinned particles, single crystals, cubes, nanorods, and nanowires.[15] Evaluation of temperature as a variable over a range of temperatures from 145 to 160 °C led to no appreciable change in morphology. However when we switched from a heating mantle to an oil bath as our heat source we saw a significant improvement in nanowire selectivity. (Figure 9) The plasmon absorption had a clear maximum at 390 nm. During the initial injection phase of the reaction the addition of the ambient temperature solutions of $AgNO_3$ and PVP to an equal volume of preheated ethylene glycol caused a rapid temperature drop. For the reactions where the temperature of the reaction was controlled using a mantle heater and the thermocouple placed in the flask there was a ten-degree drop in temperature followed by a quick recovery. The reactions where the flask and thermocouple were immersed in the oil bath the reaction temperature had twenty-degree temperature drop and did not recover until after the injection was complete.

The synthesis of nanowires is typically viewed as a two-step process of seeding and seed growth followed by uniaxial growth.[10] These results suggest that having a cooler temperature during the seeding process aides in the selectivity of wire formation. It has been shown that two sizes of nanoparticles can form at high temperatures in the presence of seed particles and that the growth of the larger particles occurs with disappearance of the smaller particles.[13] The selectivity for the larger wire-precursor particles may be enhanced at lower temperatures, possibly due to kinetic effects which favor growth from a seed

[11] Sun, Y.; Yin Y.; Mayers, M.T.; Herrisck, T. Xia, Y. *Chem Mater.*, **2002**, 14, 4736.
[12] Wiley, B.; Herricks, T., Sun Y., and Xia, Y. *Nano. Lett.* **2004**, *4*, 1733.
[13] Wiley, B.; Sun, Y.; and Xia, Y. *Langmuir.* **2005,** *21*, 8077
[14] Korte, K. E.; Skrabalek, S. E.; Xia, Y. *J. Mater. Chem.* **2008,** *18*, 437
[15] Wiley, B.; Sun, Y.; and Xia, Y. *Acc. Chem. Res* **2007,** *40*, 1067

particle[13,15,16] and that multiply twinned particles represent the thermodynamically most stable morphology.[13,17]

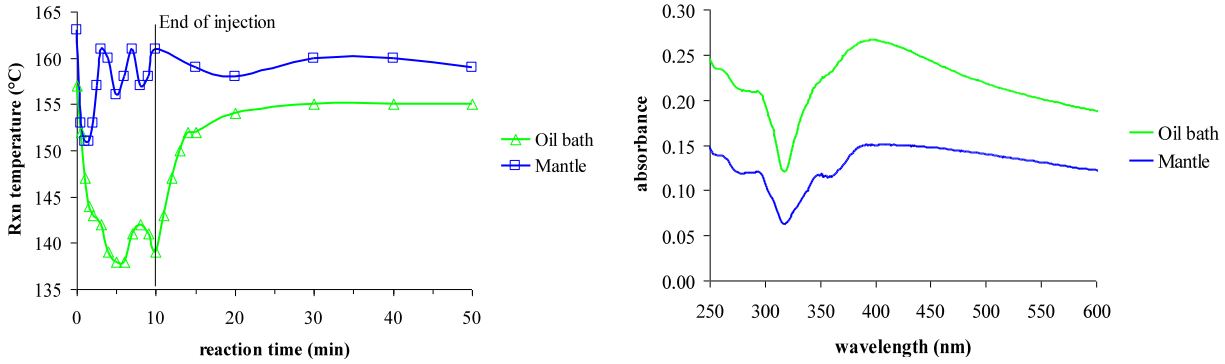

Figure 8 *Left* – Effect of heat source on the process temperature. *Right* – Effect of heat source on the absorption spectrum.

We next turned to added salts as a means of controlling morphology. The role of salts in controlling morphology is complex. Platinum chloride added to the reaction solution is believed to provide seed particles of platinum that promoted growth of multiply twinned particles[10a,13]. The presence of $FeCl_3$[13] or $CuCl_2$[14] is used as an oxygen scavenger and the chloride from NaCl serves as an etchant for the more reactive crystal twin boundaries.[14] With such a wide array of behaviors from the salts and the apparent role of oxygen as an additional etchant we decided we needed a more controlled system focusing on only three variables, PVP concentration, PVP molecular weight, and NaCl concentration. By running all our reactions under an atmosphere of either argon or nitrogen we reduced the contribution of oxygen to any etching processes alleviating the need for iron or copper salts. We chose NaCl as our "seed" salt because we reasoned the NaCl would be insensitive to oxygen in our stock solutions and therefore stable over the course of our investigations. The presence of NaCl also seemed to reliably lead to nanowires in the literature. Interestingly the apparent amount of NaCl necessary for wire formation in the literature was only 0.06 mM or approximately 3.2 ppm.[14]

From work we had done previously we knew that laboratory glassware could easily supply sufficient sodium to make controlling the amount of sodium in the reaction difficult. All glassware and stirbars were acid washed with 0.1 M nitric acid and rinsed with deionized water. Furthermore, we decided to distill our ethylene glycol to remove trace amounts of ionic contaminates and stored the freshly distilled ethylene glycol and the glycol solutions in plastic bottles previously rinsed with deionized water. Fractional distillation of ethylene glycol gave a low boiling cut that came over from 190-194 °C probably due to the presence of water. This cut was discarded and the fraction boiling at 195 °C was retained for our experiments.

It can be seen from the plasmon absorption spectrum that the reaction using distilled ethylene glycol failed to give a significant amount of nanowires. (Figure 10) Adding NaCl (0.2 mM) in the PVP solution caused a significant shift the peak maximum from 445 nm for the freshly distilled ethylene glycol to 385 nm for the reaction with added NaCl. Repeating these conditions gave an identical absorption spectrum. A drop of the reaction solution was deposited on a metal stud and analyzed by SEM. The image showed substantially pure nanowires that were approximately 20 μm long and 200 nm

[16](a) Almeida, M.; Alcacer, L. *J. Crystal Growth.* **1983,** *62*, 183. (b) Iguchi, M.; Murase, I. *J. Crystal Growth.* **1974,** *24/25*, 596. (b) Sun, Y.; Yin, Y.; Mayers, M. T.; Herricks, T. and Xia, Y. *Nano Lett.* **2003,** *3*, 955.
[17] (a) Ajayan, P. M.; Marks, L. D. *Phys. Rev. Lett.* **1998,** *60*¸ 585. (b) Marks, L. D. *Rep. Prog. Phys.* **1994,** *57*, 603. (c) Clevland, C.; Landman, U. *J. Chem. Phys.* **1991,** *94*, 7376.

in diameter giving an aspect ratio of about 100:1. (Figure 11) These wires were significantly larger in diameter than those reported in the literature that were more commonly between 50 and 100 nm. The reason for this difference is possibly due to a slight deficiency in PVP that would generate thicker wires.[11] It has also been reported that the nature of the salt can dramatically affect the wire diameter.[18]

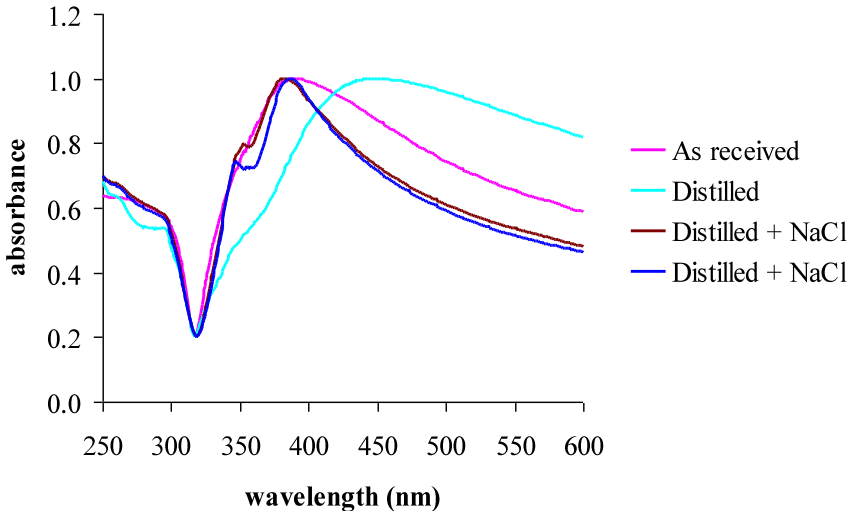

Figure 9 Effects of distillation and salt on the absorption spectrum.

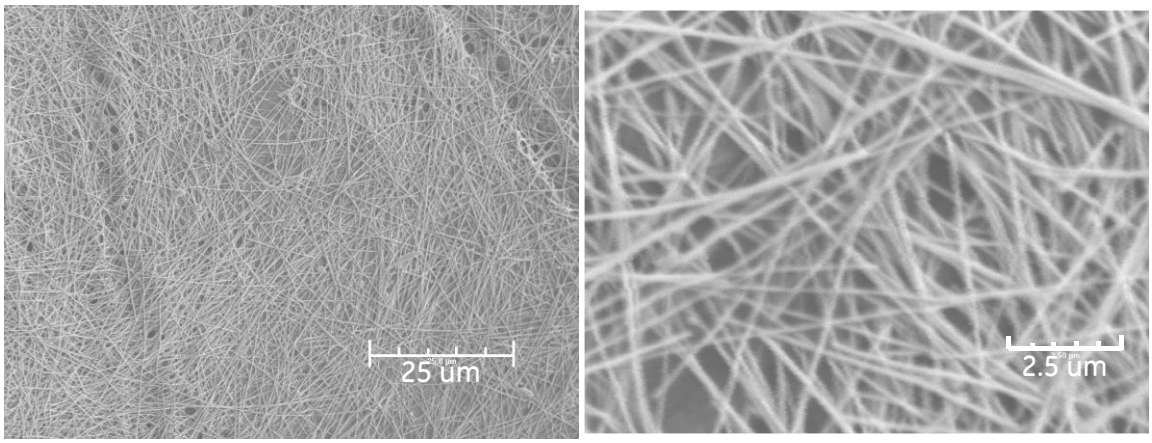

Figure 10 SEM image of nanowire reaction solution.

Attempts at further optimizing the synthesis by balancing the NaCl and PVP concentrations resulted in a new optimal set of conditions. We found that reducing the PVP concentration by 63% (0.38 M) while increasing the NaCl concentration (0.3 mM) of the literature conditions gave the sharpest plasmon absorption spectrum. These conditions were then used for scaling up the synthesis by a factor of ten in terms of the amount of $AgNO_3$. A direct scale-up seemed difficult, as we were unsure if we could supply the large volume of injection solutions at an appropriate rate or how well the reaction would

[18] Chen, C.; Wang, L.; Jiang, G.; Zhou, J.; Chen, X.; Yu, H.; Yang, Q. *Nanotechnology.* **2006,** *17,* 3933

recover from the associated temperature drop. It was decided to increase the concentrations of the injection solutions to reduce the injected volume and compensating by increasing the volume of preheated reaction solution. Under these alternate conditions the scale-up batch failed to give selective nanowire formation and we attempted to re-optimize the procedure. The optimum conditions for the large-scale reaction were only slightly different from what we had found for the small-scale reactions. An aliquot of the reaction solution was deposited on a metal stud and analyzed by SEM. The absorption spectrum was nearly identical to that of the small-scale reaction. (Figure 12)

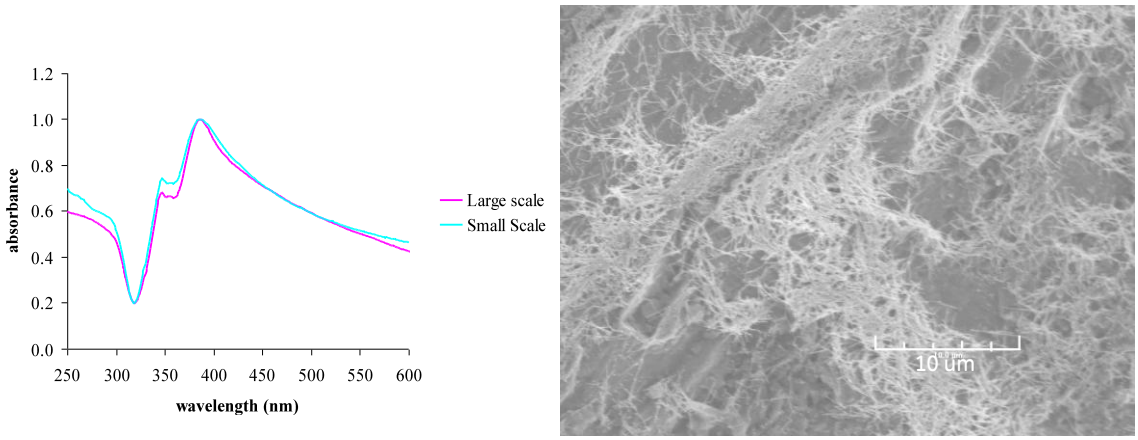

Figure 11 Absorption spectrum and SEM image of large scale nanowire synthesis

The majority of the sample was composed of short thin nanowires measuring about 80 nm in diameter and 5 μm long with small amounts large particles. Surprisingly, the new batch of wires was significantly thinner than the previous batches yet this was not reflected in a shift in the maximum absorbance to shorter wavelengths. We were interested in determining if we could achieve longer wires in the larger scale reactions and decided to run a design of experiments looking again at the concentrations of PVP, NaCl and the molecular weight of the PVP. Twelve of the reactions gave significant quantities of nanowires as determined by their absorption spectrum ten of which were analyzed by SEM for length and diameter. The data obtained from these 10 are summarized in Table 2. The average wire diameter varied between 70 to 110 nm while the length spanned 5 to 20 microns. Unlike Chen et. al., we were unable to demonstrate a correlation between the maximum absorption wavelength and either of the wire dimensions. There did appear to be a clear correlation between the width and the length of the wires. A plot the length versus width of the nanowires showed a correlation although it was not linear.

Table 2 Size analysis of nanowires with variations of [PVP], [NaCl] and PVP molecular weight.

Reaction	Polyvinylpyrrolidone mw (kDaltons)	[PVP] (M)	[NaCl] (mM)	Radius of nanowires (nm)	st. dev.	Length of nanowires (μm)	st. dev.
1	55	2.2	1.4	90	16	7	3.7
2	55	2.2	1.6	79	14	6	4.3
3	55	2.3	1.5	81	9	7	4.0
4	55	2.4	1.4	106	15	12	6.6
5	55	2.4	1.6	73	12	3	1.6
6	1000	2.2	1.4	74	10	6	2.9
7	1000	2.2	1.6	72	12	6	3.9
8	1000	2.3	1.5	97	21	7	7.1
9	1000	2.4	1.4	108	30	19	11.8
10	1000	2.4	1.6	105	23	10	10.3

Analysis of the data using Design-Expert® software showed that the concentration of PVP and NaCl both were playing a role in determining the length of the wires whereas only the concentration of PVP affected the wire width. The molecular weight of the PVP had no effect on the width of the wires in the region tested. (Figure 13)

$$(length)^{-2.4} = 1.8\times10^{-8} - 8.2\times10^{-9} * [PVP] - 6.7\times10^{-9} * [NaCl] + 3.3\times10^{-9} * [PVP] * [NaCl] \quad \text{Eq. 1}$$

$$width = -169 + 114 * [PVP] \quad \text{Eq. 2}$$

It is important to note that with the limited sample set we had we looked only at main effects and first-order interactions and that more complex effects may not have been seen. According to the analysis we needed to further decrease the NaCl concentration and increase the PVP concentration to achieve longer wires. This is in good agreement with the SEM analysis that showed large particles typical of a deficiency in PVP. Even though we may have been able to further optimize the synthesis we had generated enough good quality product to proceed with the processing of the nanowires into scattering films.

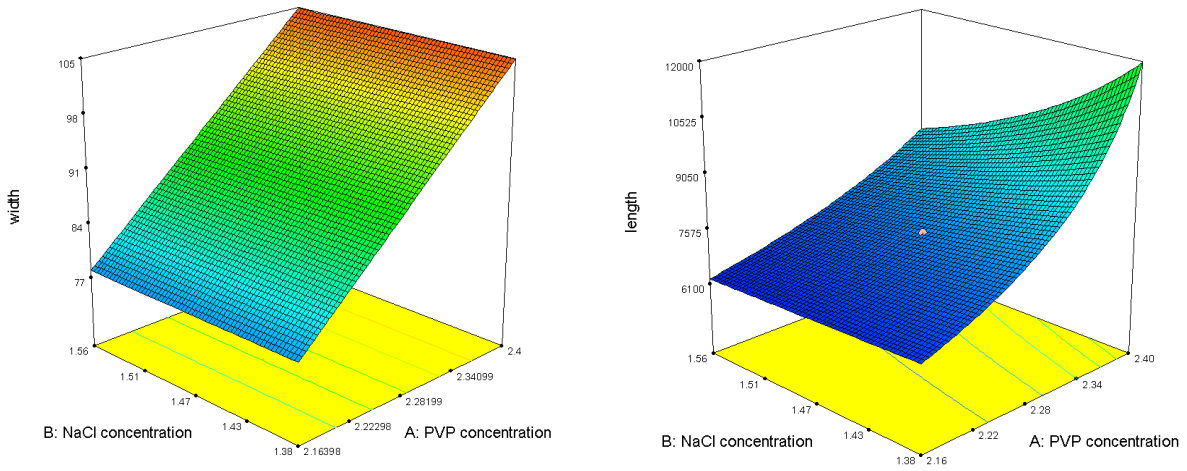

Figure 12. Surface plot of transfer functions for width *(left)* and length *(right)* as functions of NaCl and PVP concentration.

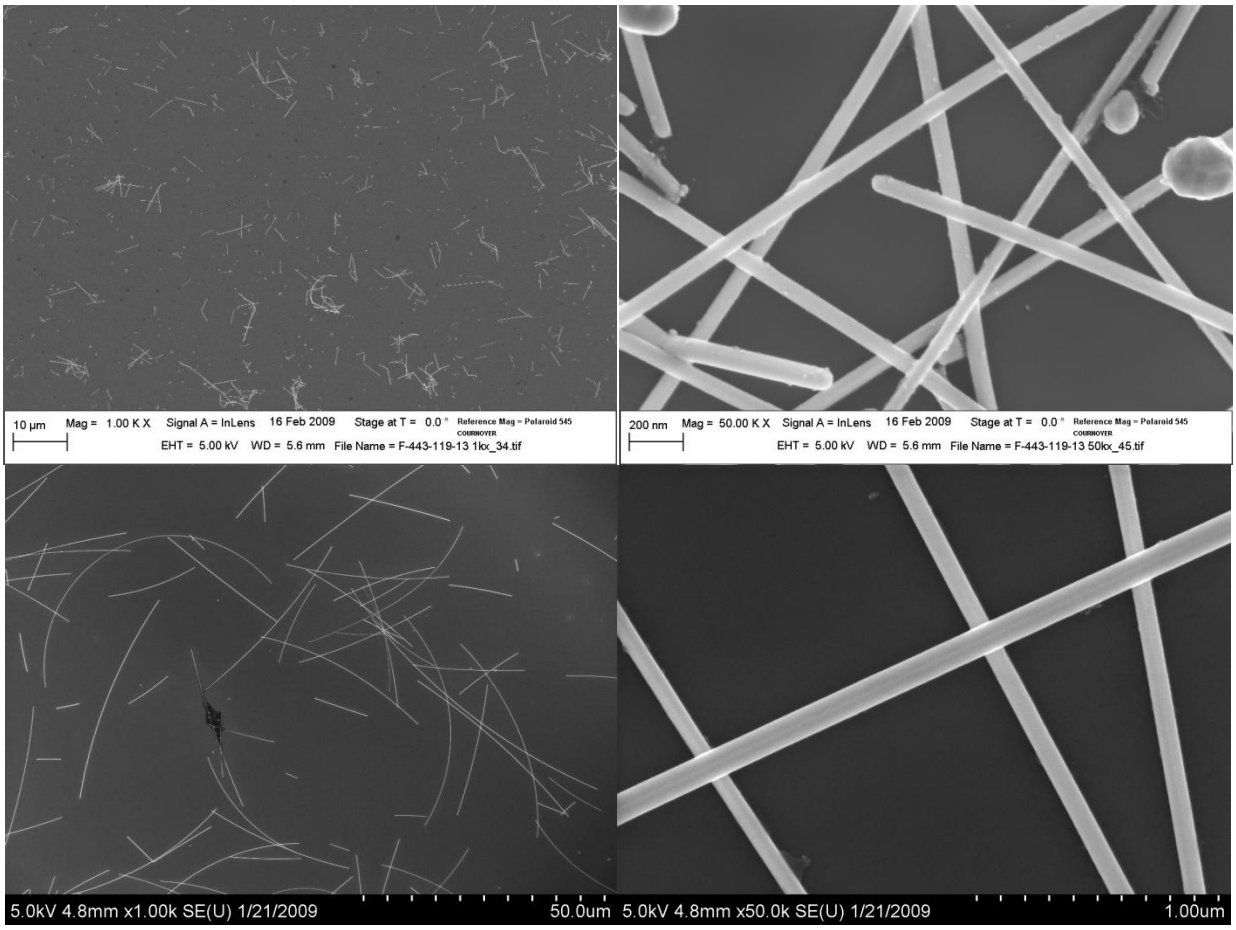

Figure 13. SEM images of reaction 5 *(top)* and 9 *(bottom)* showing short and long wires.

Silver nanowires isolated in the usual way were redispersed in 2 mL of iso-propanol and blended into acrylate solutions to give formulations containing approximately 160 ppm silver. The refractive index of the coating was determined to be 1.65. Although the intent was to build fully functional OLED devices with the scattering layer contained within the device, between the substrates rather than on top of one, we reasoned we could evaluate the efficacy of the technique using a simplified device structure. The test structure contained only a transparent substrate, the scattering layer and a layer of fluorescent polymer. Small samples were prepared by depositing the nanowire-doped resin onto a cleaned substrate and compression molding to the desired thickness. The surface of the mold imparts roughness onto the acrylate coating surface characteristic of how the mold itself was made.

Scheme 1. Process for preparing coated substrates using different coating techniques.

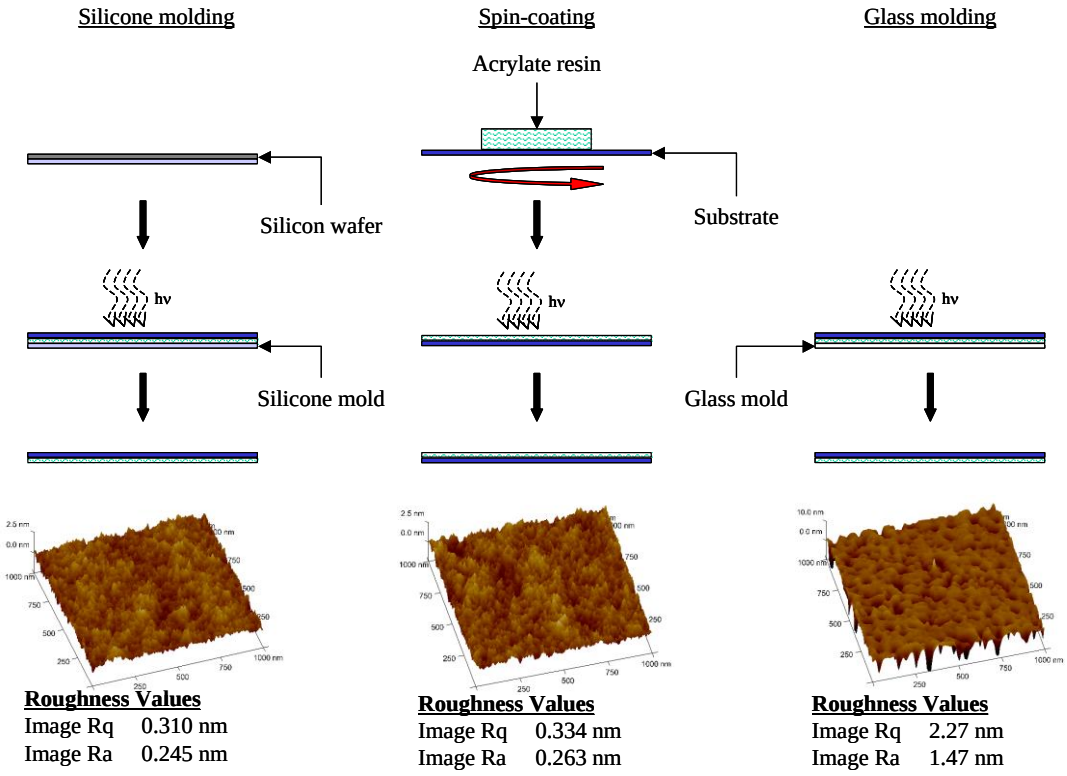

Characterization of the coating surfaces by AFM showed that silicone molds made using silicon wafers provided acrylate coatings with a roughness comparable to control coatings prepared by spin-coating the acrylate. Coatings prepared using polished glass molds were significantly rougher than either silicone mold or spin-coated samples. (see Scheme 1) Analysis of the samples by UV-visible microscopy showed a decrease in transmitted light. This was expected and by subtracting the spectrum of the undoped sample we find the plasmon absorption spectrum characteristic of silver nanowires. The shift in wavelength maximum is due primarily to a change in the refractive index of the medium of the sample although we cannot rule out aggregation of the wires. (Figure 15)

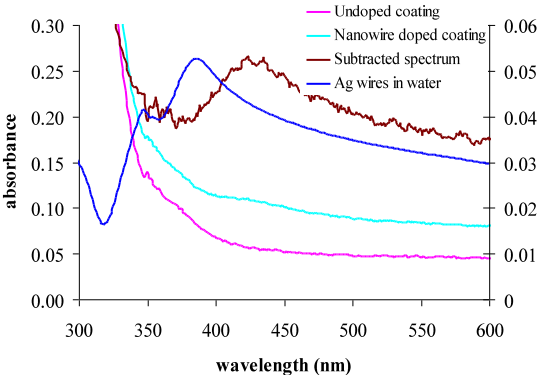

Figure 14. Absorption spectrum of coated glass *(left axis)*. Difference spectrum and nanowire spectrum *(right axis).*

We also examined the nanowire-doped samples using optical microscopy. While the wires have nanometer scale in one dimension they are tens of microns in length rendering them visible under non-polarized light. In the image we see what appear to be wires on the order of 0.5 mm long roughly 25 times the average size found in the SEM analysis. Figure (16) Agglomeration of the wires into bundles could account for the apparent size discrepancy between the two methods.

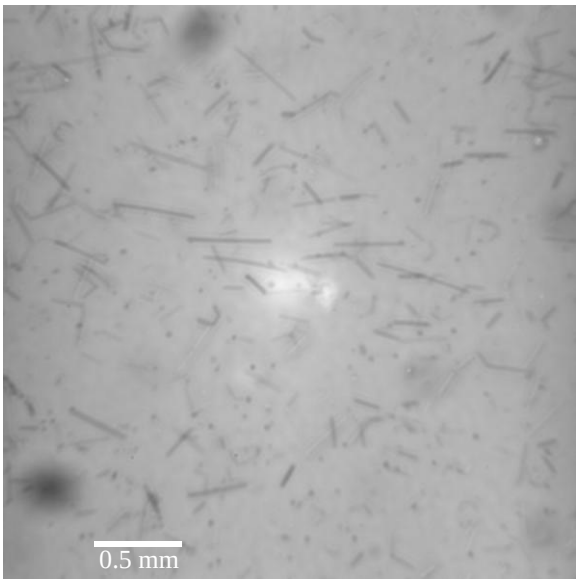

Figure 15 Optical image of nanowire doped coating.

Samples made using silicone molding were further coated with blue fluorescent polymer and gave samples suitable for fluorimetry. In our experiments we were interested in looking at high refractive index substrates such as polyethylene naphthalate (PEN). A high refractive index substrate should more strongly couple to the emissive polymer layers and further enhance the light output. We found that PEN strongly absorbed light out to 400 nm, much longer than the glass or PET based samples in which the acrylate coating began strongly absorbing at 350 nm. (Figure 17) For this reason we used 410 nm excitation in our experiments.

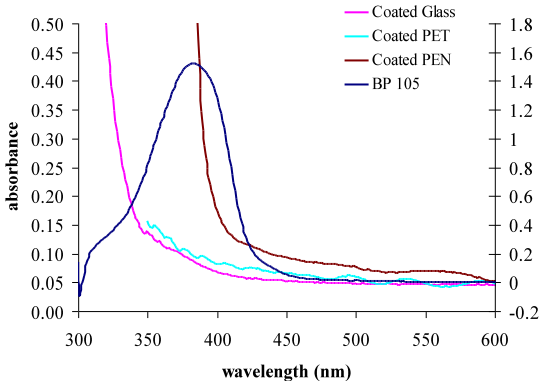

Figure 16 Absorption spectrum of coated substrates *(left)* and BLUE *(right)*.

Fluorescence from the test samples was compared to a glass slide coated with acrylate without nanowire doping. The fluorescence intensity was corrected to account for variations in the optical density of the blue polymer layer. The ratio of fluorescence intensity between the test samples and the glass

control is the output coupling factor. Control samples containing two levels of YAG particles were run for comparison. In this test the silver nanowire doped samples directed 1.8 times as much light out of the device compared to samples containing no wires. These techniques were extended to large 5" x 5" plastic substrates suitable for OLED device testing and were submitted for ITO deposition. We are awaiting the results of these tests.

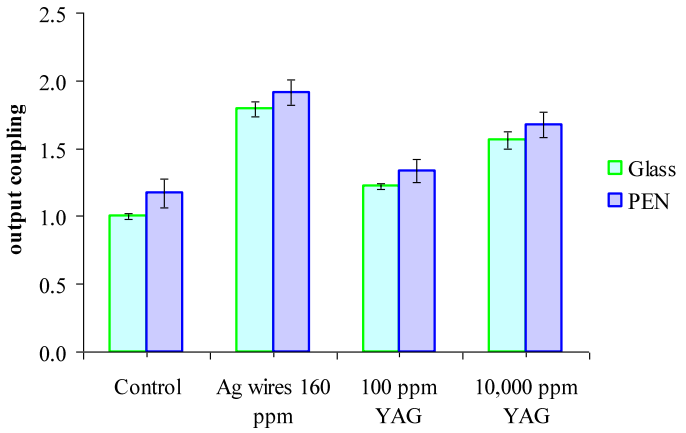

Figure 17 Effect of different embedded light scattering materials on light output.

Summary

Silver nanowires were successfully synthesized using a polyol process and used as light scattering particles in a high refractive index acrylate hardcoat on PEN substrates. The performance of the scattering layer on small samples using a test architecture showed an increase in light output by a factor of ~1.8. The parameters of PVP and NaCl concentration, reaction temperature and PVP molecular weight were explored. A set of preliminary transfer functions relating the wire dimensions to PVP and NaCl were determined. The results indicated that further optimization to provide larger wires should be possible. We have incorporated these nanowires into high index of refraction coatings on PEN substrates. The effect of molding on the roughness of the hardcoat was examined and it was found that the coatings are smooth. Preliminary tests of these coatings indicate that they can potentially improve the amount of light extracted from OLED devices.

Task 3 –

During the program the use of higher reflectivity cathodes was extensively examined, both from a theoretical perspective and an experimental one. The advantage of this approach is that it requires only modest changes in the OLED design and does not introduce morphology into the OLED structure that can lead to leakage issues. A number of material approaches were considered, and a material system was examined that would enable a higher reflectivity cathode. Using the known dielectric properties of the system the net light extraction can be calculated and compared to the standard cathode design. Following the flow process indicated in Figure 6, the total light output is calculated using both a microcavity model to calculate the total amount of light injected into the substrate and the angular distribution of the light as it is injected into the substrate. A typical 4 layer solution processed device design was used as input to perform these calculations. As an additional output, the microcavity model also predicts a total reflectivity. The results of these calculations are shown in Table 3.

Table 3 Output of microcavity model for a typical OLED design used in the program.

		Standard cathode	High Reflectance cathode
In device	Air	.22	.19
	Substrate	.42	.43
	Device	.14	.08
	Plasmon	.22	.30
		Transmission to substrate	
		82%	91%
		52.4% top inj (substrate+air)	56.4% top inj (substrate+air)

The second part of the calculation is then to calculate the total light output in the presence of a light scattering film. The result of these calculations is shown in Table 4. The fraction of light coupled into the substrate is taken from the previous table (Table 3). The optical scattering model (Figure 5) is used to calculate the total light output, which sets an upper limit on the device EQE. The results of this calculation indicate that for this device design, while there is a small difference in the total amount of light that is injected into the substrate, there is a large difference in the total amount of light that is coupled out of the device in the presence of a light scattering film. The reason for this may be readily understood. In the limit of perfectly reflective OLED and a non-absorbing scattering film, all the light that is coupled into the substrate will eventually be coupled out into the air. In the opposite limit, where the OLED is black, then the presence of light scattering actually reduces the total amount of light output, as light is redirected toward the lossy OLED. Thus, *optical loss is a key parameter for all light outcoupling schemes and must be carefully managed and minimized.* The improvements projected by the analysis shown in Table 4 are quite significant, enough to improve a 60 LPW OLED into a 75 LPW OLED system. It should be noted however, that the overall calculated improvement is sensitive to the device input parameters, and is closer to 10% in some device configurations.

Table 4 Calculation of the total maximum possible EQE for a typical OLED design used in the program

	Standard	High Reflectance
Fraction coupled into substrate	0.524	0.564
Out coupling to air	0.67	0.81
Net max EQE	0.35	0.46

A second key part of the effort was to demonstrate the practicality of this scheme for increasing the light output. A number of test devices were built using higher reflectivity cathode design. The reflectance of the OLEDs was measured at a single reflectance angle of incidence ~ 20^{o}. The incident beam was a white light spectrum, set to mimic the spectral characteristics of the typical white light OLED constructed during the project. Typically the measured reflectivity of the OLED with a standard cathode was 0.71 +/- .04 (one sigma deviation) and the measured reflectance of the high reflectance cathode system, was 0.82 +/- 0.03. Great care was taken to ensure the gauge repeatability and reproducibility (GR&R) of the home built apparatus, and the instrument had a demonstrated precision of +/- 0.01 based on GR&R analysis; thus the observed variability in OLED reflectance is largely `due to the underlying

variability of the cathode process. These measured values of the reflectivity are broadly consistent with the calculated values of the reflectivity using the microcavity model.

Functional OLEDs were constructed with a high reflective cathode. Consistently across all device builds the EQE of the device was observed to increase, typically by about 10%. In addition, once the cathode process was optimized, there did not appear to be a voltage penalty associated with the high reflectivity cathode design. Thus the increases in the observed EQE led directly to increases in the measured LPW. Thus the improvement is quite 'generic' and should work for almost any OLED design.

The high reflectance cathode does have somewhat demanding process tolerances, and requires specific tooling to properly control and execute. Thus the final process was not scalable to large area batch coating without significant re-tooling, however, that the necessary tooling requirements can be incorporated into future acquisitions.

Task 4

There are three main challenges to transition an OLED technology from the laboratory scale to the larger area required: minimizing the resistive losses associated with moving current through the thin conductive oxide film, minimizing losses associated with defects, and finally establishing a robust process that minimizes the part to part variance. All of these requirements are much harder to meet using plastic substrates since the typical ITO conductivites are lower, the substrate is softer and can delaminate layers upon flexing, and is not as dimensionally stable as glass. As a result a considerable portion of the project effort was devoted to meeting these challenges in order to meet the final deliverable total lumen output requirement.

One method to address the issue of resistive loss was demonstrated by GE under DOE program DE-FC26-00NT40989, which is to use a series interconnected device, in which many small area elements are monolithically coupled in series on the substrate. This has the advantage that in addition to addressing the resistance loss problem, a degree of device robustness is incorporated, as a failure in a single small element does not lead to failure of the entire series connected string. This approach comes at the cost of requiring patterning of the organic layers, attention to ensuring that the series interconnection area is free of residue and a tight degree of dimensional alignment is required between the patterned anode, the patterned organic layers and the patterned cathode. An alternate approach is to provide an extensive series of high-conductivity metallic bus lines over the entire ITO substrate. This approach tends to be somewhat simpler to fabricate and has a greater dimensional tolerance, at the cost of a loss of defect tolerance. Which approach is used depends upon the available tooling for pattering, and the extent to which shorting defects can be minimized. During the program both approaches were used, with a bus line approach selected for the final deliverable, due to its relative simplicity and the fact that the shorting defects were minimized to an acceptable level.

Of particularly high concern was leakage in the OLED emissive areas. Leakage in OLEDs can vary continuously from an additional high resistance pathway that diminishes the efficiency of an emitting element to a completely shorted, non-emissive element. The degree to which these leakage paths occur drives many of the choices of the device layout, series and parallel electrical architecture, and hence the final appearance of the device. Central to effective control is measurement and characterization. Two primary routes of leakage characterization will be used, the standard current and light versus voltage measurement and high resolution thermal imaging. Thermal imaging of the thin film devices is a well-established technique, and under pulsed conditions with lock-in detection, is capable of resolving mK temperature differences. [Breitenstein 2004] In an infra-red image, process induced shorts appear as bright hot spots. The ability to connect thermal images with specific device structures and processing conditions allowed formulation of effective strategies to reduce leakage and other loss mechanisms such

as parasitic resistance pathways that lead to hot spots in the integrated panel. (Figure 19)The information obtained from the analysis of these images formed an important part of the design selection process.

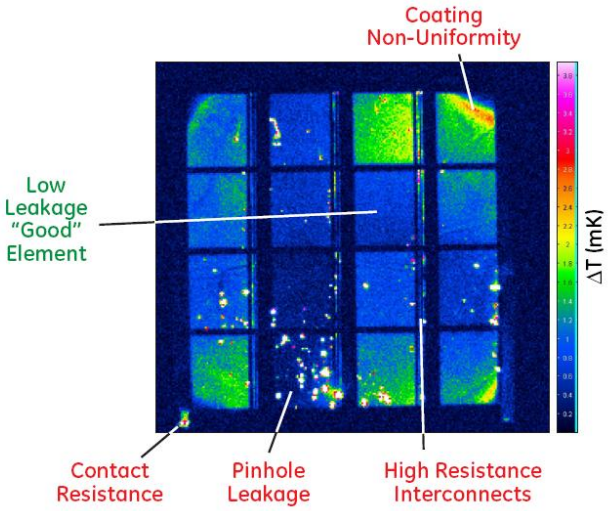

Figure 18: A means of detecting shorting and other types of defects in OLED devices. Shown is a differential infra-red image of an operating OLED device obtained by lock-in-thermometry. The labels indicate the assignment of the observed hot areas to different failure mechanism within the device.

Once the ultimate process and OLED design was chosen larger scale production runs could begin. An important step in this process was to ensure that the EQE of a large area device had similar performance as small area device of similar material composition and layer design. Figure20 shows that this goal was achieved.

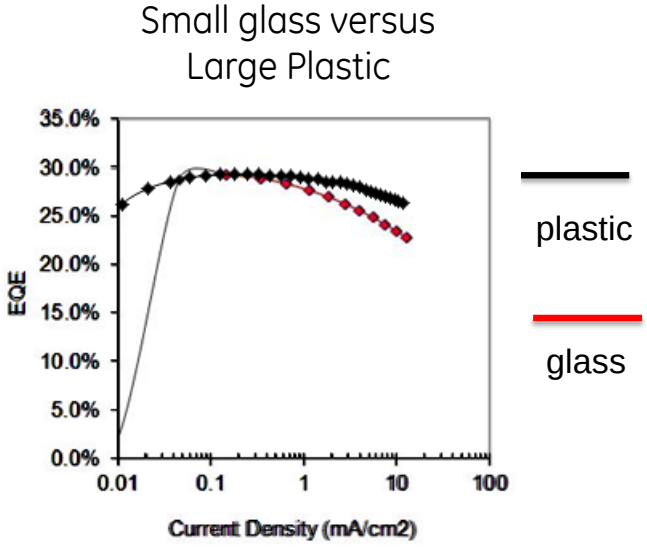

Figure 19: Comparison of the EQE performance of similar OLEDs built on large area plastic (3"x6") versus small area glass (1"x1") substrates.

The devices used to make the final luminaire, shown in Figures 2 and 21, were solution processed under clean room conditions using batch processing of small molecules. All devices were encapsulated to prevent water and oxygen ingress, and after several months in the laboratory ambient do not appear to be significantly degraded by eye. After encapsulation, the devices remained sufficiently flexible to conform to curved supports. Several "runs" were required to produce the necessary cohort of devices used for incorporation into the final deliverable. Although a final manufacturing process even for pre-pilot scale will deviate considerably from the process used to make the deliverable prototype, the ability to minimize the variance of a set of samples provides an important demonstration of the ability to manufacture OLED on plastic. Thus the construction of the necessary cohort of devices is an important first step understanding the relationship between the product vision of Figure 1 and the technical realities of scaling up the design. The statistics obtained over the 40 element cohort of devices included in the luminaire are shown in Table 5. The table lists average LPW , external quantum efficiency (EQE), energy efficiency (watts optical/ watts electrical) W/W, the CIE color coordinates, the estimated CRI and distance above the black body locus (dBB), the phosphor efficiency or lumens per optical watt radiated (LPWr) and the central wavelength of emission. The LPW is calculated as the product of the w/w energy efficiency and the LPWr.

Since the dBB is slightly above the BB curve, the CRI estimate is high. This is a function of the particular emitter blend chosen. During the project it was found that the dBB can be reduced as more red emitter is incorporated by changing the dye composition, which will also reduce the CRI down to about 80 and decrease the LPWr to about 300. In the table both an overall standard deviation of the entire cohort and pooled standard deviation in which devices are grouped by run are reported. The pooled standard deviation provides an estimate of the within run or short term variability and the total standard deviation provides an estimate of longer term, run-to-run variability. The fact that the long term variability is not much larger than the pooled standard deviation provides additional support for the robustness of the process with respect to the efficiency metric.

Table 5 Summary of performance of the OLED panels used in the final OLED luminaire.

	at 1000cd/m2									
	LPW	EQE	W/W	CIEx	CIEy	CCT	CRI	dBB	LPWrad	nm center
Average	46.0	27.8%	14.6%	0.454	0.447	3052	87.2	0.038	314.5	592
STDEV all	3.8	1.55%	1.00%	0.009	0.004	157	2.04	0.0064	7.9	3
STDEV all (%)	8.2%	5.6%	6.9%	1.9%	1.0%	5.1%	2.3%	16.9%	2.5%	0.5%
STDEV pooled	2.7	1.48%	0.85%	0.002	0.000	36.4	0.15	0.000928	1.2	1
STDEV pooled (%)	5.9%	5.3%	5.8%	0.5%	0.1%	1.2%	0.2%	2.4%	0.4%	0.1%

The variability of the large area lifetime is much harder to ascertain, due to the much smaller number of samples available for the destructive lifetest. In general it was observed that run-to-run lifetime variability was much larger than the variability in LPW. The longest lived large area white devices have T_{70} operating lifetimes of several hundred hours. The best large area T_{50} lifetimes of the devices are well over 1000 hours.

The OLED panels were integrated on to larger 3/32" Lexan ™ sheets to form conformable large area luminaires. These luminaire were powered by standard LED power supplies (Thor Labs model LEDD1B). The luminaire is held in shape by a thin (2" high) sheet metal strip at the bottom. An additional picture of one of the flexible luminaire panels appears in Figure 21.

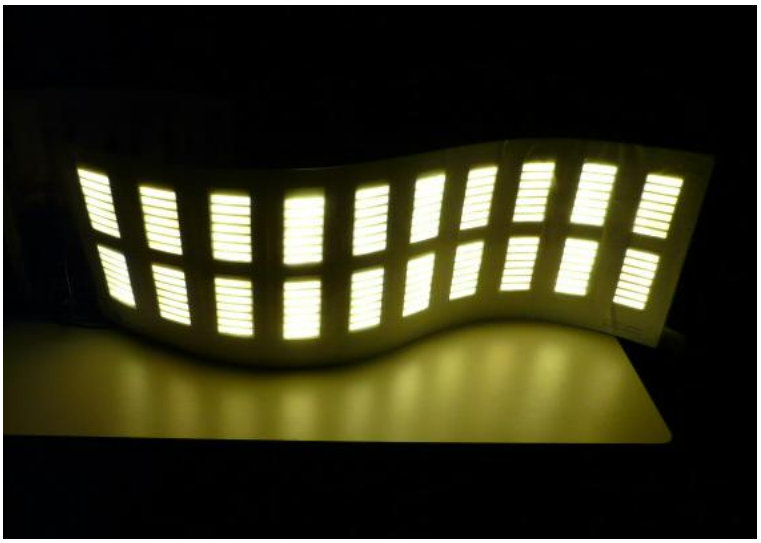

Figure 20 View of the one luminaire panel delivered by the program

IV. Conclusions and Recommendations

The overall goal of the program was to apply improvements in light outcoupling technology to a practical large area plastic luminaire, and thus enable the product vision of an extremely thin form factor high efficiency large area light source. The target substrate was plastic and the baseline device was operating at 35 LPW at the start of the program. The target LPW of the program was a >2x improvement in the LPW efficacy and the overall amount of light to be delivered was relatively high 900 lumens. Despite the extremely difficult challenges associated with scaling up a wet solution process on plastic substrates, the program was able to make substantial progress. A small molecule wet solution process was successfully implemented on plastic substrates with almost no loss in efficiency in transitioning from the laboratory scale glass to large area plastic substrates. By transitioning to a small molecule based process, the LPW entitlement increased from 35 LPW to 60 LPW. A further 10% improvement in outcoupling efficiency was demonstrated via the use of a high reflecting cathode, which reduced absorptive loss in the OLED device. The calculated potential improvement in some cases is even larger ,~30%, and thus there is considerable room for optimism in improving the net light coupling efficacy, provided absorptive loss mechanisms are eliminated. Further improvements are possible if scattering schemes such as the silver nanowire based hard coat structure are fully developed. The wet coating processes were successfully scaled to large area plastic substrate and resulted in the construction of a 900 lumen luminaire device using OLEDs that had an average initial operating performance of 46 LPW.

Some of the key findings from the program are the critical importance of developing and using the correct metrics to quantify and measure improvements in light outcoupling. Use of EQE ratio metrics such as an “enhancement factor”, which is a highly problematic practice, should be avoided. A second finding is the critical importance of eliminating absorptive loss mechanisms. Simply by increasing the reflectivity of the OLED device, the efficacy of light extraction using scattering films increases quite dramatically. Developing tooling that enable high reflectance cathodes should be a specification of the cathode process. Elimination of absorptive loss in other layers e.g. hole injection layer and electron injection layer materials is also highly desirable. A third finding is the importance of diagnosing leakage mechanisms and prevalence in large area devices, IR lock-in thermometry is a particularly useful tool in this regard. Finally, we observe very little difference between the luminous efficacy of OLEDs built on plastic versus glass substrates, even at large area, which leads optimism to unique OLED product vision of ultra-thin large area emissive light sources.